Scaling and Statistics in Three-Dimensional Compressible Turbulence

Jianchun Wang,[1] Yipeng Shi,[1] Lian-Ping Wang,[2] Zuoli Xiao,[1] X. T. He,[1] and Shiyi Chen[1,*]

[1]*SKLTCS and CAPT, College of Engineering, Peking University, Beijing 100871, China*

[2]*Department of Mechanical Engineering, University of Delaware, Newark, Delaware 19716, USA*

(Received 9 November 2011; published 25 May 2012)

The scaling and statistical properties of three-dimensional compressible turbulence are studied using high-resolution numerical simulations and a heuristic model. The two-point statistics of the solenoidal component of the velocity field are found to be not significantly different from those of incompressible turbulence, while the scaling exponents of the velocity structure function for the compressive component become saturated at high orders. Both the simulated flow and the heuristic model reveal the presence of a power-law tail in the probability density function of negative velocity divergence (high compression regime). The power-law exponent is different from that in Burgers turbulence, and this difference is shown to have a major contribution from the pressure effect, which is absent in the Burgers turbulence.

DOI: 10.1103/PhysRevLett.108.214505 PACS numbers: 47.27.−i, 47.40.−x, 47.53.+n

Compressible three-dimensional (3D) fluid turbulence is of great importance to a large number of industrial applications and natural phenomena, including high-temperature reactive flows, transonic and hypersonic aircrafts, interplanet space exploration, and star-forming clouds in galaxies [1]. An accurate description (e.g., subgrid-scale stress modeling [2]) of small-scale compressible turbulence is desired when modeling complex compressible turbulence. In this Letter, we study the effects of compressibility and shock discontinuities on the statistics of fluid turbulence, with specific attention to the similarity and difference between 3D compressible turbulence and one-dimensional Burgers turbulence.

Since it is difficult to analyze 3D compressible turbulence, Burgers [3] first systematically studied a nonlinear model of fluid turbulence; i.e., the one-dimensional Burgers equation. Since then, the one-dimensional Burgers turbulence has frequently been investigated theoretically and numerically [4–13]. According to multifractal theory [4], isolated shocks connected by smooth ramps lead to bifractal scaling exponents of the velocity structure function in the Burgers turbulence. Mitra *et al.* [5] performed simulations of one-dimensional Burgers turbulence with up to 2^{20} mesh points to study the multiscaling of velocity structure functions. They found that scaling exponents asymptotically saturate to one with increasing orders. Much effort has also been made to exploit the asymptotic behavior at the tail of the probability density function (PDF) of the negative velocity derivative in Burgers turbulence [7–13]. E *et al.* [10] predicted that the large negative velocity gradients stem mainly from preshocks, leading to the $-7/2$ power-law tail in the PDF of negative velocity gradients (provided that preshocks do not cluster). Bec [11] verified this result using a novel particle and shock tracking numerical method. Boldyrev, Linde, and Polyakov [12] carried out simulations of random forced Burgers turbulence using a standard shock capturing scheme. They obtained a power-law exponent of about -3.4, very close to the theoretical value of -3.5.

Compared to incompressible turbulence, 3D compressible turbulence is more complex due to nonlinear interactions between solenoidal and compressive modes of velocity fluctuations and couplings between the velocity field and pressure field [14]. Besides the vortex-filament induced intermittency observed in the incompressible turbulence, shock waves in the compressible turbulence add an intermittent dissipation mechanism of different topological structures [15]. Schmidt, Federrath, and Klessen [16] studied the two-point velocity statistics of compressible turbulence at a root-mean-square (rms) Mach number of 5.5 by numerical simulations of Euler equations. A universal scaling has been recovered by reformulation of the refined similarity hypothesis in terms of the mass-weighted velocity $\rho^{1/3}\boldsymbol{u}$. They also reported that the most intermittent dissipative structures were shocks, due to extreme compressibility of the flow field. Galtier and Banerjee [17] derived an exact relation for correlation functions in compressible isothermal turbulence that mimics the Kolmogorov $4/5$ law in the incompressible isotropic turbulence. Consequently, they theoretically revealed the effect of dilation and compression on the local energy transfer. By dimensional arguments, they further obtained a $k^{-5/3}$ spectrum of the density-weighted velocity $\rho^{1/3}\boldsymbol{u}$.

Here, a forced compressible turbulence is simulated in a cubic box with periodic conditions at 1024^3 grid resolution, using a novel hybrid approach described in [18] [also see Supplemental Material [19]]. A total of 20 flow fields at the statistical stationary stage spanning $2.68 \leq t/T_e \leq 4.63$ are extracted to analyze the flow statistics, where t is time and T_e is the large eddy turnover time defined by $T_e = \sqrt{3}L/u'$, where L is the integral length scale and u' is the rms velocity magnitude. The turbulent Mach number is $M_t = u'/\langle c \rangle = 1.03$, where $\langle c \rangle$ is the average sound speed,

and the Taylor microscale Reynolds number is $R_\lambda = 254$. The rms velocity divergence is found to be $\theta' = 0.35\omega'$, where ω' is the rms vorticity magnitude. It is also found (not shown in the Letter) that power spectra for velocity $\mathbf{u}$, and density-weighted velocities $\rho^{1/3}\mathbf{u}$ and $\rho^{1/2}\mathbf{u}$ almost overlap, indicating a minor effect of density fluctuations on the velocity spectrum.

In order to reveal the underlying physics in the compressible turbulence, we employ the Helmholtz decomposition [14]; namely, the fluid velocity $\mathbf{u}$ is decomposed into a solenoidal component $\mathbf{u}^s$ and a compressive component $\mathbf{u}^c$: $\mathbf{u} = \mathbf{u}^s + \mathbf{u}^c$, where $\nabla \cdot \mathbf{u}^s = 0$ and $\nabla \times \mathbf{u}^c = 0$. In our simulated flow, the ratio of rms fluctuations, $u^{c\prime}/u^{s\prime}$, is found to be 0.22, comparable to 0.18 reported in Porter, Pouquet, and Woodward [20] at a similar turbulent Mach number.

Figure 1 shows the normalized PDFs of the longitudinal increments, $\Delta u^s(r) \equiv \Delta \mathbf{u}^s(\mathbf{r}) \cdot \mathbf{r}/r$, of the solenoidal velocity component at different separations, where $\mathbf{r}$ is the separation vector and $r = |\mathbf{r}|$. The PDFs exhibit stretched exponential tails at small spatial separations and approach Gaussian as the separation increases. These trends are very similar to those found in incompressible turbulence [21]. Figure 2 shows the normalized PDFs of the longitudinal increments, $\Delta u^c(r) \equiv \Delta \mathbf{u}^c(\mathbf{r}) \cdot \mathbf{r}/r$, of the compressive velocity component. The shapes of the PDFs are highly skewed at small separations and always have a longer tail than Gaussians for all separations. In addition, at the one-grid-length separation the PDF has a power-law tail with an exponent of -2.5 on the left side. We note that, due to the power-law behavior of the PDF tail, when the viscosity asymptotically approaches zero, special care is required since the variance of the velocity increment may become unbounded. Similar results have been reported for Burgers turbulence. In the random-force driven Burgers turbulence, the PDFs of velocity increments have an algebraic tail on the left side, leading to strong intermittency and bifractality of the scaling exponents [8].

We plot the normalized PDFs of the pressure increments Δp in Fig. 3. The shapes of these PDFs are nearly symmetric and have longer tails at small spatial separations than those in the incompressible turbulence at the same Taylor Reynolds number (also see [22]). The pressure changes drastically in the high compression regime, leading to intensive pressure increments at small separations. Power-law tails are also found in the pressure-increment PDF at the one-grid-length separation, with a power-law exponent of -3.

The scaling exponents for the longitudinal structure functions in the inertial subrange are defined as

$$S^L_{s,n}(r) \equiv \langle |\Delta u^s(r)|^n \rangle \sim r^{\zeta^L_{s,n}}, \quad (1)$$

$$S^L_{c,n}(r) \equiv \langle |\Delta u^c(r)|^n \rangle \sim r^{\zeta^L_{c,n}}, \quad (2)$$

where $\zeta^L_{s,n}$ and $\zeta^L_{c,n}$ are the scaling exponents for the two velocity components, respectively. Our results show that $\zeta^L_{s,n}$ agrees well with those from the incompressible turbulence [23,24]. This implies that at $M_t \sim 1$, the two-point statistics of the solenoidal velocity component are insensitive to the presence of shocks. In addition, similar to results in [20,25], we find that the scaling exponents of the full velocity $\mathbf{u}$ are also the same as those in the incompressible turbulence. However, the scaling exponents of the compressive velocity component, shown in the inset of Fig. 4, is drastically different. A saturation of $\zeta^L_{c,n}$ is observed for $n \geq 5$, and the saturated value is estimated to be $\zeta^L_{c,\infty} \approx 0.7$. The compensated longitudinal structure functions at orders 5 and 6 are shown in Fig. 4, where the separation is normalized by the Kolmogorov length η. According to the multifractal theory, the saturation of exponents is caused by the domination of frontlike structures [25]. Benzi *et al.* [25] observed that the density field displays frontlike structures, leading to saturation of the scaling exponents for density structure functions in a weakly compressible turbulence at rms Mach number 0.3. However, for the velocity field, they did not find any difference between weakly compressible turbulence and incompressible

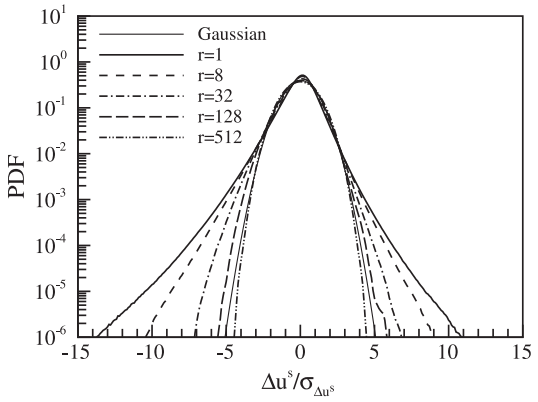

FIG. 1. Normalized probability density functions of Δu^s.

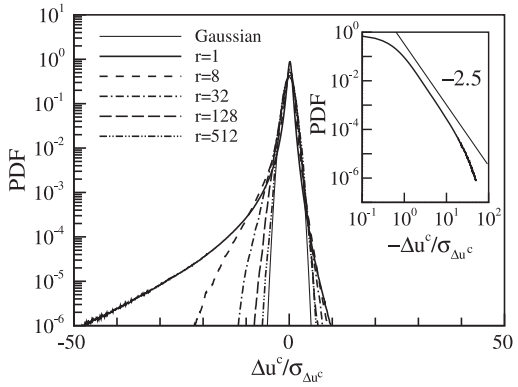

FIG. 2. Normalized probability density functions of Δu^c. Inset: log-log plot of the same PDF for the negative Δu^c at the one-grid-length separation.

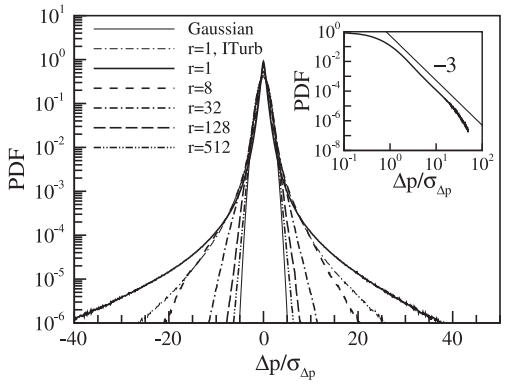

FIG. 3. Normalized probability density functions of Δp. Thin dash-dotted line is the corresponding PDF at the one-grid-length separation for incompressible turbulence (ITurb) at the same Taylor Reynolds number. Inset: log-log plot of the PDF for positive Δp in compressible turbulence at the one-grid-length separation.

turbulence. On the other hand, due to a relatively higher turbulent Mach number in our simulated flow, shocks produce a significant number of frontlike structures in the compressive velocity field, causing saturation of scaling exponents $\zeta^L_{c,n}$. Furthermore, substantial uncertainties in the exponents at high orders are associated with large temporal fluctuations, which ascribe to instability of intermittency structures [26].

The PDF of velocity divergence (Fig. 5) exhibits a power-law tail for large negative divergences and a super-exponential tail for large positive divergences, both qualitatively similar to the PDF of the velocity derivative in Burgers turbulence [13]. In Burgers turbulence with infinitesimal viscosity, the large negative velocity gradients stem mainly from preshocks, leading to the power-law tail in the PDF of negative velocity gradients [10]. In the compressible turbulence, through studying the contours of velocity divergence (not shown here), we have identified that the power-law regime of velocity divergence has a major contribution from preshocks and weak shocklets rather than strong shock waves. Otherwise, the power-law exponent for the PDF of velocity divergence is -2.5, the same as that for the PDF of the longitudinal increments of the compressive velocity component at the one-grid-length separation but qualitatively different from the power-law exponent (-3.5) for the PDF of the velocity gradient in one-dimensional Burgers turbulence. To understand this difference, we write down the equation of the velocity derivative in Burgers turbulence [9]:

$$\frac{\partial \xi}{\partial t} + u\frac{\partial \xi}{\partial x} = -\xi^2 + \nu\frac{\partial^2 \xi}{\partial x^2} + \frac{\partial f}{\partial x}, \tag{3}$$

where $u(x, t)$ is the velocity and $\xi(x, t)$ is the velocity gradient. The forcing $f(x, t)$ is used to maintain the Burgers turbulence to be statistically stationary. In contrast, the governing equation for velocity divergence in 3D Navier-Stokes flow is

$$\frac{\partial \theta}{\partial t} + u_j\frac{\partial \theta}{\partial x_j} = -\frac{\partial u_j}{\partial x_i}\frac{\partial u_i}{\partial x_j} - \frac{1}{\gamma M^2}\frac{\partial}{\partial x_i}\left(\frac{1}{\rho}\frac{\partial p}{\partial x_i}\right) + \frac{4\nu_0}{3Re}\frac{\partial^2 \theta}{\partial x_i^2}. \tag{4}$$

To simplify the discussions, we have neglected the effect of density fluctuations on the viscous term. It is seen that there are some similarities between the term $\frac{\partial u_j}{\partial x_i}\frac{\partial u_i}{\partial x_j}$ in Eq. (4) and ξ^2 in Eq. (3), the former causing strong skewness of the PDF of velocity divergence provided that the turbulent Mach number is larger than 0.3 [27].

Below, we demonstrate how the pressure term alters the power-law exponent of the PDF of velocity divergence in the high compression regime. Following the similar procedure provided by Gotoh and Kraichnan [6], we can derive the Liouville equation for the PDF of velocity divergence $P(\theta)$ as follows (see Supplemental Material [19]):

$$\frac{\partial P}{\partial t} - \frac{\partial(\theta^2 P)}{\partial \theta} - \theta P + D = F, \tag{5}$$

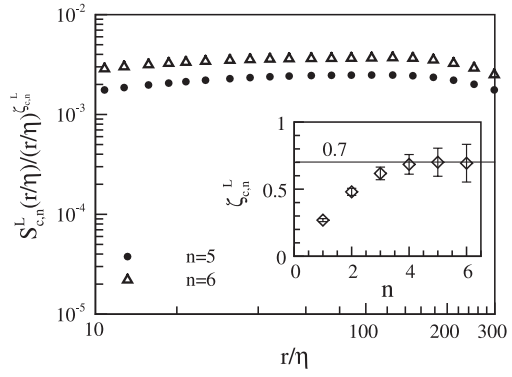

FIG. 4. Compensated structure functions for $n = 5$ and $n = 6$ as a function of normalized separation. Inset: scaling exponents $\zeta^L_{c,n}$ as a function of n. The separation r is normalized by the Kolmogorov length scale $\eta = [\langle\nu\rangle^3/\epsilon]^{1/4}$, where ν is the kinematic viscosity and ϵ is the average kinetic energy dissipation rate [14].

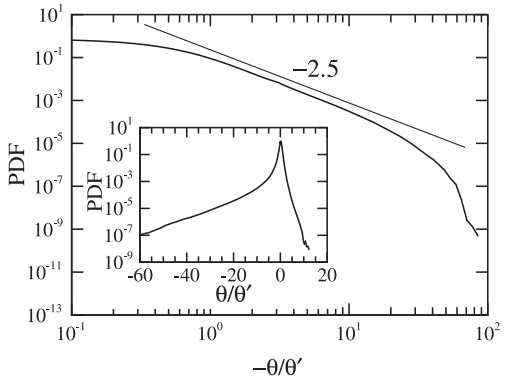

FIG. 5. Probability density function of velocity divergence.

where the dissipation term is

$$D(\theta) = \frac{4\nu_0}{3Re}\frac{\partial}{\partial\theta}\left[\left\langle \frac{\partial^2\theta}{\partial x_i^2}\,\middle|\,\theta\right\rangle P\right] \quad (6)$$

and the *forcing* term, including effects of pressure and anisotropic straining, is

$$F = \frac{\partial}{\partial\theta}\left[\left\langle \frac{1}{\gamma M^2}\frac{\partial}{\partial x_i}\left(\frac{1}{\rho}\frac{\partial p}{\partial x_i}\right) + \left(\frac{\partial u_j}{\partial x_i}\frac{\partial u_i}{\partial x_j} - \theta^2\right)\,\middle|\,\theta\right\rangle P\right]. \quad (7)$$

This equation is written formally the same as the PDF equation of velocity derivative in Burgers turbulence but with a different dissipation term and forcing term [13]. It has been argued previously [7–13] that Burgers turbulence has a power-law tail in the PDF of ξ for the high compression regime. If Burgers turbulence is driven by large scale white-in-time random forcing, this tail is believed to be universal with an exponent -3.5 in the limit of vanishing viscosity. Other exponents are possible if Burgers turbulence is driven by forcing with prescribed power-law spectra [8].

In Fig. 6, we plot the average normalized straining $\frac{1}{\theta'^2}\times\frac{\partial u_j}{\partial x_i}\frac{\partial u_i}{\partial x_j}$ conditioned on the velocity divergence as a function of velocity divergence. For the compression regime (i.e., $\theta<0$), we find that the straining term can be well approximated by $\frac{\theta^2}{\theta'^2}$, implying that the effect of stretching-tilting dynamics on the PDF of velocity divergence is small. In addition, its compressive component $\frac{1}{\theta'^2}\frac{\partial u_j^c}{\partial x_i}\frac{\partial u_i^c}{\partial x_j}$ dominates the overall straining term. These interesting approximations are consistent with the numerical simulations that show that intensive velocity gradients are dominated by variations in one spatial direction during compression in the shock waves [14,28]. Therefore, the solenoidal velocity component has very limited contribution to the PDF equation of velocity divergence in the compression regime. In contrast, in the expansion regime (i.e., $\theta>0$), the straining term is no longer close to the square of the divergence. Based on dimensional analysis, the anisotropic straining term $[\frac{1}{\theta'^2}\frac{\partial u_j}{\partial x_i}\frac{\partial u_i}{\partial x_j}-(\frac{\theta}{\theta'})^2]$ can be represented by the square of the divergence multiplied by a nondimensional constant. Figure 6 shows that this nondimensional constant is around -0.8 in the expansion regime instead of almost zero in the compression regime. The conditional straining is always positive, implying that the magnitude of the velocity divergence is increased by the straining when $\theta<0$, but it is decreased by the straining when $\theta>0$. However, the magnitude of the conditional straining for $\theta>0$ is only about $1/5$ of the values for $\theta<0$, indicating that the effect of straining on the velocity divergence is substantially weaker in the expansion regime. Therefore, the role of the straining term in Eq. (4) is similar to that of the ξ^2 term in Eq. (3) in the compression regime due to shock structures, but in the expansion regime it is weakened by relaxation of multidirectional advection and by the solenoidal velocity dynamics, where the flow is dominated by vortex structures.

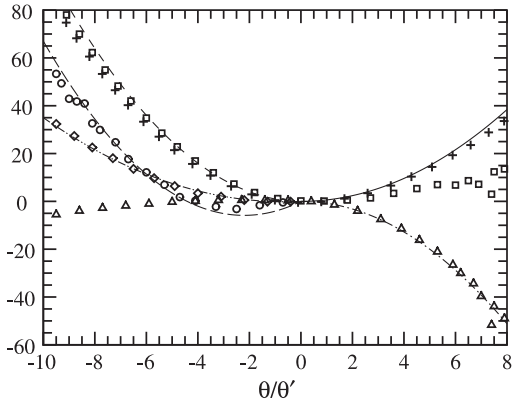

FIG. 6. Conditional average of $\langle\frac{1}{\theta'^2}\frac{\partial u_j}{\partial x_i}\frac{\partial u_i}{\partial x_j}|\frac{\theta}{\theta'}\rangle$ (squares), $\langle\frac{1}{\theta'^2}\times\frac{\partial u_j^c}{\partial x_i}\frac{\partial u_i^c}{\partial x_j}|\frac{\theta}{\theta'}\rangle$ (plusses), $\langle\frac{1}{\theta'^2}\frac{\partial u_j}{\partial x_i}\frac{\partial u_i}{\partial x_j}-(\frac{\theta}{\theta'})^2|\frac{\theta}{\theta'}\rangle$ (triangles), $\langle\frac{1}{\theta'^2}\frac{4\nu_0}{3Re}\times\frac{\partial^2\theta}{\partial x_i^2}|\frac{\theta}{\theta'}\rangle$ (diamonds) and $\langle\frac{1}{\theta'^2}\frac{1}{\gamma M^2}\frac{\partial}{\partial x_i}(\frac{1}{\rho}\frac{\partial p}{\partial x_i})|\frac{\theta}{\theta'}\rangle$ (circles). The lines represent $\alpha(\frac{\theta}{\theta'})^2+\beta\frac{\theta}{\theta'}$ with $(\alpha,\beta)=(1.0,0.0)$ (dashed line), $(\alpha,\beta)=(0.6,0.0)$ (solid line), $(\alpha,\beta)=(-0.8,0.0)$ (dash-dotted line), $(\alpha,\beta)=(0.4,0.5)$ (dash-dot-dotted line) and $(\alpha,\beta)=(1.2,5.3)$ (long dashed line).

We now focus our discussion on the PDF equation in the strong compression regime where the power-law tail appears. In Fig. 6, we show average values of the viscous term and pressure term conditioned on θ in the PDF equation. As also shown in the figure, the anisotropic staining effect is small compared with the other two terms and may be neglected. The viscous term is well fitted by a parabola $\alpha_\nu(\frac{\theta}{\theta'})^2+\beta_\nu\frac{\theta}{\theta'}$ with $\alpha_\nu=0.4$ and $\beta_\nu=0.5$. A similar procedure was suggested by Gotoh and Kraichnan [9] based on an analysis of the viscous term inside an equilibrium single shock in Burgers turbulence. The pressure term can also be approximated by a parabola with coefficients $\alpha_p=1.2$ and $\beta_p=5.3$. With these approximations, we obtain the following solution at the stationary stage:

$$P(\theta) = C_0\theta^{-1}\left[\theta+\frac{(\beta_\nu-\beta_p)}{1+\alpha_p-\alpha_\nu}\right]^{-1-[1/(1+\alpha_p-\alpha_\nu)]}. \quad (8)$$

It follows that, for large negative θ, $P(\theta)\propto\theta^{-q}$, where $q=2+\frac{1}{1+\alpha_p-\alpha_\nu}$. Using the fitting values for α_p and α_ν, we then obtain $q=2.56$. This is very close to the value of 2.5 shown in Fig. 5. An exponent of -3 is obtained without considering the pressure term and viscous term, which is consistent with the case of Burgers turbulence [13]. The viscous term enlarges the exponent as in Burgers turbulence [13]. The key difference here is the modification of the power-law exponent from the pressure term. We note that the role of the pressure is opposite to that of the viscosity in determining this exponent, and the effect of pressure predominates.

Finally, we emphasize that the viscosity is small, but finite, in our discussion on the PDF of velocity divergence.

Several issues require further investigations, including the relative contributions of preshocks and weak shocklets to the power-law tail of the PDF at higher Reynolds numbers, the asymptotic behavior of the power-law exponent in the limit of vanishing viscosity, and the effect of Mach number on the power-law behavior.

We thank Qionglin Ni, Zhenhua Xia, and Zhou Jiang for many useful discussions. This work was supported by the National Natural Science Foundation of China (Grants No. 10921202 and No. 91130001) and the National Science and Technology Ministry under a subproject of the 973 program (Grant No. 2009CB724101). Simulations were done on a cluster computer at the Center for Computational Science and Engineering at Peking University, China and on Bluefire at NCAR, USA through CISL-35751014 and CISL-35751015. L.-P. W. acknowledges support from the National Science Foundation under Grants No. ATM-0730766 and OCI-0904534.

*syc@pku.edu.cn

[1] P. Padoan and A. Norlund, Astrophys. J. **576**, 870 (2002).
[2] B. Kosovic, D. I. Pullin, and R. Samtaney, Phys. Fluids **14**, 1511 (2002).
[3] J. M. Burgers, in *Advances in Applied Mechanics* (Academic, New York, 1948), Vol. 1, p. 171.
[4] E. Aurell, U. Frisch, J. Lutsko, and M. Vergassola, J. Fluid Mech. **238**, 467 (1992).
[5] D. Mitra, J. Bec, R. Pandit, and U. Frisch, Phys. Rev. Lett. **94**, 194501 (2005).
[6] T. Gotoh and R. H. Kraichnan, Phys. Fluids A **5**, 445 (1993).
[7] A. M. Polyakov, Phys. Rev. E **52**, 6183 (1995).
[8] A. Chekhlov and V. Yakhot, Phys. Rev. E **52**, 5681 (1995); V. Yakhot and A. Chekhlov, Phys. Rev. Lett. **77**, 3118 (1996).
[9] T. Gotoh and R. H. Kraichnan, Phys. Fluids **10**, 2859 (1998).
[10] W. E, K. Khanin, A. Mazel, and Y. Sinai, Phys. Rev. Lett. **78**, 1904 (1997).
[11] J. Bec, Phys. Rev. Lett. **87**, 104501 (2001).
[12] S. Boldyrev, T. Linde, and A. Polyakov, Phys. Rev. Lett. **93**, 184503 (2004).
[13] J. Bec and K. Khanin, Phys. Rep. **447**, 1 (2007).
[14] R. Samtaney, D. I. Pullin, and B. Kosovic, Phys. Fluids **13**, 1415 (2001).
[15] L. Pan, P. Padoan, and A. G. Kritsuk, Phys. Rev. Lett. **102**, 034501 (2009).
[16] W. Schmidt, C. Federrath, and R. Klessen, Phys. Rev. Lett. **101**, 194505 (2008).
[17] S. Galtier and S. Banerjee, Phys. Rev. Lett. **107**, 134501 (2011).
[18] J. Wang, L.-P. Wang, Z. Xiao, Y. Shi, and S. Chen, J. Comput. Phys. **229**, 5257 (2010).
[19] See Supplemental Material at http://link.aps.org/supplemental/10.1103/PhysRevLett.108.214505 for a brief description of the hybrid simulation approach used in the Letter and a derivation of the PDF equation governing velocity divergence.
[20] D. Porter, A. Pouquet, and P. Woodward, Phys. Rev. E **66**, 026301 (2002).
[21] S. Chen, G. D. Doolen, R. H. Kraichnan, and Z. She, Phys. Fluids A **5**, 458 (1993).
[22] N. Cao, S. Chen, and G. D. Doolen, Phys. Fluids **11**, 2235 (1999).
[23] Z. S. She and E. Lévêque, Phys. Rev. Lett. **72**, 336 (1994).
[24] N. Cao, S. Chen, and Z. S. She, Phys. Rev. Lett. **76**, 3711 (1996).
[25] R. Benzi, L. Biferale, R. T. Fisher, L. P. Kadanoff, D. Q. Lamb, and F. Toschi, Phys. Rev. Lett. **100**, 234503 (2008).
[26] S. Chen and N. Cao, Phys. Rev. Lett. **78**, 3459 (1997).
[27] S. Pirozzoli and F. Grasso, Phys. Fluids **16**, 4386 (2004).
[28] J. Wang, Y. Shi, L.-P. Wang, Z. Xiao, X. He, and S. Chen, Phys. Fluids **23**, 125103 (2011).